Paleoceanography and Paleoclimatology

AGU ADVANCING EARTH AND SPACE SCIENCE

RESEARCH ARTICLE
10.1029/2022PA004484

Expansion of Reducing Marine Environments During the Ireviken Biogeochemical Event: Evidence From the Altajme Core, Gotland, Sweden

Brittany M. Stolfus[1], Lindsi J. Allman[2], Seth A. Young[2], Mikael Calner[3], Emma R. Hartke[4], Stephan C. Oborny[5], Alyssa M. Bancroft[6], and Bradley D. Cramer[1]

[1]Department of Earth and Environmental Sciences, University of Iowa, Iowa City, IA, USA, [2]Department of Earth, Ocean and Atmospheric Sciences, National High Magnetic Field Laboratory, Florida State University, Tallahassee, FL, USA, [3]Department of Geology, Lund University, Lund, Sweden, [4]Department of Geosciences, Pennsylvania State University, University Park, PA, USA, [5]Kansas Geological Survey, University of Kansas, Lawrence, KS, USA, [6]Iowa Geological Survey, University of Iowa, Iowa City, IA, USA

Key Points:

- New high-resolution sulfur isotope data show the expansion of reducing environments during the onset of the Ireviken Biogeochemical Event
- Reducing environment expansion began prior to the onset of Ireviken positive carbon isotope excursion
- Compilation of data from Laurentia and Baltica suggest this may have been a global redox event

Correspondence to:
B. M. Stolfus,
brittany-stolfus@uiowa.edu

Citation:
Stolfus, B. M., Allman, L. J., Young, S. A., Calner, M., Hartke, E. R., Oborny, S. C., et al. (2023). Expansion of reducing marine environments during the Ireviken Biogeochemical Event: Evidence from the Altajme core, Gotland, Sweden. *Paleoceanography and Paleoclimatology*, *38*, e2022PA004484. https://doi.org/10.1029/2022PA004484

Received 24 MAY 2022
Accepted 9 FEB 2023

Abstract New $\delta^{34}S_{py}$ (pyrite) and $\delta^{34}S_{CAS}$ (carbonate-associated sulfate) across the Llandovery-Wenlock boundary (~432 Ma) provide evidence for the expansion of reduced marine environments during the Ireviken Biogeochemical Event. This event consists of a major positive carbon isotope excursion, increased biotic turnover, and other major perturbations and changes within biogeochemical cycles. This interval of time has been hypothesized to coincide with an expansion of reducing marine environments that caused increased organic carbon burial and led to the Ireviken positive carbon isotope excursion (ICIE). Previous high-resolution carbon isotope work in the Altajme core from Gotland, Sweden provides the highest resolution record of the ICIE yet documented and provides an ideal expanded stratigraphic section to study this event. Local expansion of reduced marine environments within the deeper shelf setting of the Altajme core is indicated by a positive shift in $\delta^{34}S_{py}$ values and increase in pyrite sulfur concentrations at the onset of the ICIE. These data are indicative of increased microbial sulfate reduction within this portion of the Baltic Basin. Combined with new $\delta^{34}S_{CAS}$ data from this core, as well as additional data from distant basins, the new data presented here suggest a global expansion of reduced environments led to an increase in organic carbon burial and the ICIE.

Plain Language Summary New sulfur isotope data from the Silurian Period (~432 Myr ago) provide evidence of low-oxygen marine environments during a major extinction event and global carbon cycle perturbation known as the Ireviken Biogeochemical Event (IBE). The high-resolution data presented here build upon recent data generated from a ~300 m long drill core recovered from the Swedish island of Gotland that records this important ancient global change event in one of the thickest and most complete stratigraphic sections available anywhere in the world. Our new high-resolution record, combined with data from other areas across the globe, demonstrate that there was likely a global expansion of low-oxygen environments in the oceans at the very onset of this biogeochemical event that played an important role in both the extinction event as well as the global carbon cycle perturbation.

1. Introduction

The Silurian Period was a dynamic interval in the history of the Earth system and contains at least seven major biogeochemical events that consist of biotic turnover, perturbations to the global carbon cycle, and other major changes within biogeochemical cycles (Cooper et al., 2014; Cramer et al., 2011; Cramer & Jarvis, 2020; Crampton et al., 2016; Melchin et al., 2020; Young et al., 2019). This interval of time (443.1–419.0 Ma) includes a unique window in the evolution of the Earth system that is after the Great Ordovician Biodiversification Event (Edwards et al., 2017; Servais et al., 2010; Webby et al., 2004) and before the development of a complete terrestrial ecosystem during the Devonian (e.g., Labandeira, 2005). Silurian marine global change events allow us to investigate biogeochemical cycling prior to the major development of the terrestrial biosphere, yet, in a window of time with fully developed marine ecosystems (Servais et al., 2010).

One of the best known and most intensively studied Silurian events is the Ireviken Biogeochemical Event (IBE) that occurred at the Llandovery-Wenlock boundary. This event was first identified as a series of stepwise extinctions in conodonts and originally referred to as the Ireviken Extinction Event (IEE; Aldridge et al., 1993;

Jeppsson, 1987, 1990, 1997a). This event also severely impacted scolecodonts, trilobites, brachiopods, and chitinozoans (Calner, 2008; Cooper et al., 2014; Crampton et al., 2016). A major positive carbon isotope excursion that typically reaches +5‰ (absolute values) referred to as the Ireviken carbon isotope excursion (ICIE) began during the IEE and persisted well into the Wenlock Epoch (Bickert et al., 1997; Cramer & Jarvis, 2020; Cramer et al., 2010a; Kaljo et al., 1997; Melchin et al., 2020; Samtleben et al., 1996). The IBE is temporally and chronostratigraphically well constrained by conodonts, graptolites, and high-precision chemical abrasion isotope-dilution thermal-ionization-mass spectrometry dates from bentonites (Batchelor & Jeppsson, 1994; Cramer et al., 2012; Jeppsson, 1997b; Kiipli et al., 2001; Männik et al., 2015; McAdams et al., 2019; Melchin et al., 2020; Munnecke et al., 2003). Whereas the timing of extinctions with respect to global carbon perturbations are well known during this interval, there remains no consensus on the driver(s) and ultimate cause(s) of the IBE.

There have been numerous causes proposed for the ICIE over the past 25 yr, however most hypotheses now focus on enhanced organic carbon sequestration and burial (Cramer & Saltzman, 2005, 2007; Hartke et al., 2021; Munnecke et al., 2003). Enhanced organic carbon burial can produce a positive carbon isotope excursion by sequestration and removal of ^{12}C from the ocean-atmosphere reservoir, thereby producing a positive $\delta^{13}C$ excursion, and thus has become the preferred mechanism to explain most major positive carbon isotope excursions (e.g., Cramer & Jarvis, 2020). Enhanced organic carbon burial can be the result of an expansion of reducing marine environments, elevated primary productivity, or a combination of both (Berner, 2006; Hayes et al., 1999; Kump & Arthur, 1999). However, the presence of a major carbon isotope excursion on its own cannot identify which of these may have been the primary driver. Sulfur isotopes can be used as a proxy for the expansion or contraction of reducing environments (e.g., Paytan et al., 2020) by a similar sequestration and removal of ^{32}S from the marine sulfate reservoir during enhanced pyrite burial. $\delta^{34}S$ records have become one of many paleoredox proxies to pair with carbon isotope chemostratigraphy to evaluate potential causative mechanisms for ancient biogeochemical events (e.g., Gill, Lyons, & Jenkyns, 2011; Gill et al., 2007, 2011; Richardson et al., 2019; Rose et al., 2019; Saltzman et al., 2011; Young et al., 2019).

Sulfur isotope data, from both carbonate-associated sulfate (CAS) and sedimentary pyrite, have begun to be produced from the IBE and many records show a perturbation to the sulfur isotope system that corresponds with the ICIE (Makhnach et al., 2016; Richardson et al., 2019; Rose et al., 2019; Young et al., 2019, 2020). However, some of these records either do not record the entire interval, were not sampled at high resolution, or show inconsistency from section to section, both regionally and globally. One outstanding question regarding the IBE is the precise temporal relationship between the extinction interval, the onset of the perturbation of the global carbon cycle, and the sulfur isotope records spanning the Llandovery-Wenlock boundary. For this study, we sampled the Altajme core for paired sulfur isotope analyses of both pyrite and CAS. This core was drilled on the island of Gotland, Sweden, specifically to obtain one of the most complete and expanded sections for the Sheinwoodian Stage ever recovered. This core was previously analyzed by Hartke et al. (2021) for high resolution (>100 samples through the duration of the ICIE) paired $\delta^{13}C_{carb}$ and $\delta^{13}C_{org}$. Here, we combine new paired sulfur isotope data with these previous carbon isotope datasets to provide a precise record of the timing and relationships between the carbon and sulfur isotopic systems during this major marine biogeochemical event in the Silurian.

1.1. Geologic Setting and Stratigraphy

The island of Gotland is an erosional remnant of the extensive carbonate platforms that formed in the interior of the Baltic Basin during the Silurian. Exposed strata are composed of open-marine shelf facies and shallow marine reef-associated deposits (Calner et al., 2005) that were formed in the Southern subtropical belt between a latitude of 10° and 20° south (Figure 1; Scotese, 2014). The extensive carbonate production that occurred through most of the Silurian on Gotland makes this an ideal locality for high-resolution sampling due to the expanded geologic record. The interior of Baltica has remained relatively stable throughout its Phanerozoic tectonic history with deformation focused primarily on the margins of the continent (Cocks & Torsvik, 2005), and there is also little to no tectonic imprint and only minor faulting with limited displacement across the island. The strata dip less than 1° to the southeast with an erosional strike from northeast to southwest. Exposed strata on Gotland include >700 m of the upper Llandovery through the Ludlow series (Jeppsson et al., 2006). The Altajme core studied here was drilled approximately 2,200 m southwest of Buttle Church in south-central Gotland and is the focus of this study (Figure 1). Lithostratigraphic data, preliminary graptolite data, and detailed chemostratigraphic data combined with a series of identifiable bentonites and biostratigraphic data from the southern Gotland Grötlingbo-1 core (Männik et al., 2015) permit precise identification of lithostratigraphic units within the Altajme core studied here.

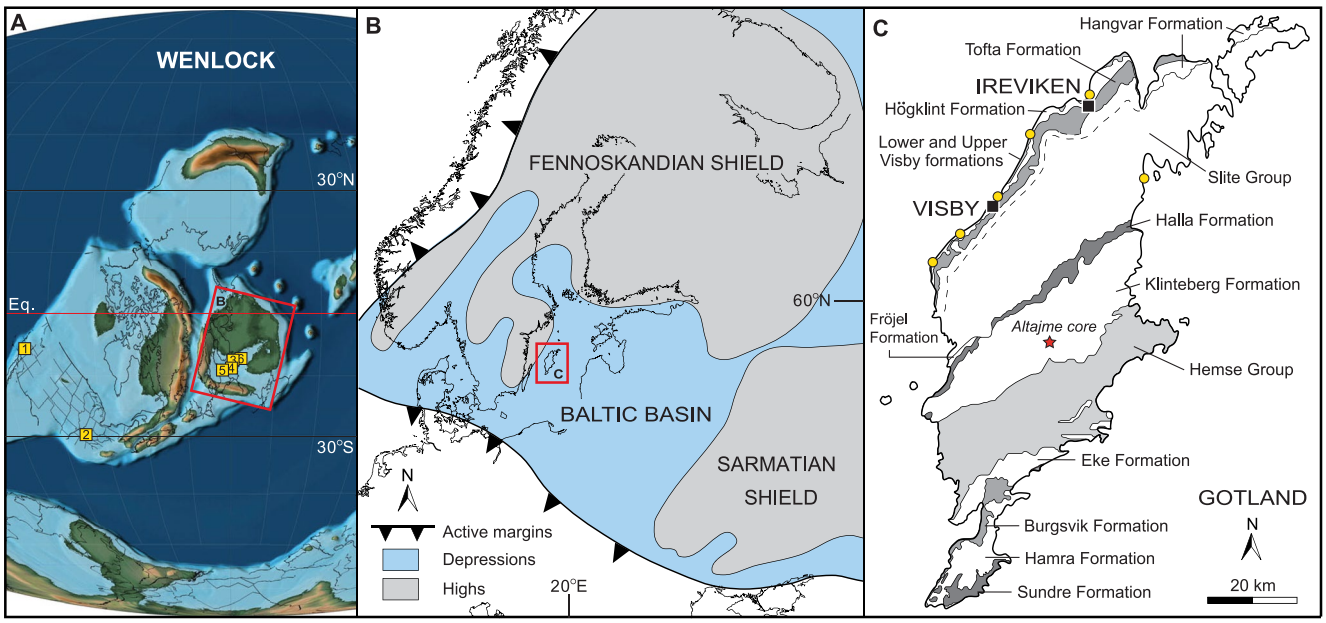

Figure 1. (a) Wenlock paleogeography (Scotese, 2014). Yellow squares illustrate data compiled in text. (1) Young et al. (2019), (2) Young et al. (2019), (3) Richardson et al. (2019), (4) Young et al. (2020), (5) Rose et al. (2019), (6) Richardson et al. (2021). (b) Map of modern-day Northern Europe showing the Baltic Basin and major emergent areas during the Silurian (modified from Baarli et al., 2003), and (c) geologic map of Gotland, Sweden (from Cramer et al., 2012) with lithostratigraphic units as well as locations of the Altajme core of this study. Yellow dots indicate the sampling localities of Rose et al. (2019). Figure modified from Biebesheimer et al. (2021).

This region has been the primary area of study for Silurian biogeochemical events and is the global reference area for the IBE. The IBE, including, stable and radiogenic isotope geochemistry and paleontology (Cramer et al., 2012, 2010a; Gelsthorpe, 2004; Hartke et al., 2021; Jeppsson, 1987, 1997a; Lehnert et al., 2010; Munnecke et al., 2003; Rose et al., 2019; Samtleben et al., 1996; Vandenbroucke et al., 2013; Wenzel & Joachimski, 1996) spans the Llandovery-Wenlock boundary (Figures 2 and 3) and has been identified in multiple localities across several paleocontinents (e.g., Jeppsson, 1997a, 1997b; McAdams et al., 2019; Melchin et al., 2020). The IBE corresponds with an extinction event in which conodont diversity decreased along with other major faunal groups including scolecodonts, trilobites, brachiopods, and chitinozoans (Aldridge et al., 1993; Calner, 2008; Jeppsson, 1987, 1990). This extinction consists of a series of extinction datums (Datums 1–8, e.g., Jeppsson, 1997a, 1997b) where the current position of the base of the Wenlock Series is essentially at Datum 2 of the IEE (Cramer et al., 2010a; Melchin et al., 2020). The corresponding positive carbon isotope excursion (ICIE) began within the extinction interval and the carbonate carbon signal

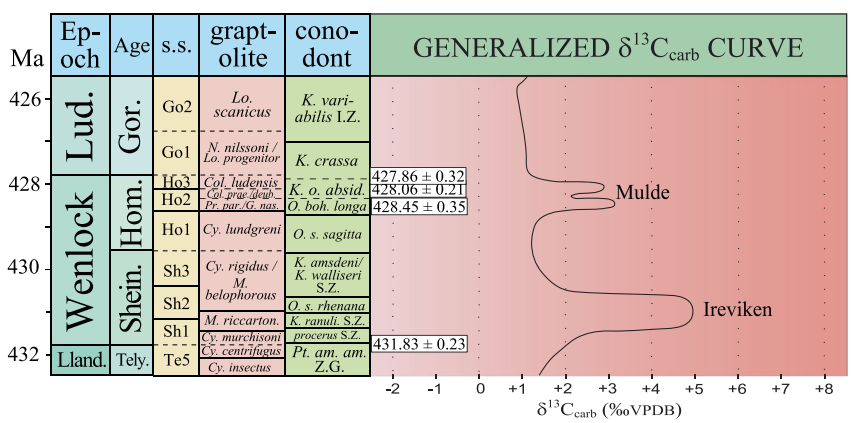

Figure 2. Silurian timescale with conodont and graptolite biozones, radioisotopic dates, and generalized carbon isotope stratigraphy. (s.s. = stage slice) Modified from original figure in McAdams et al. (2019).

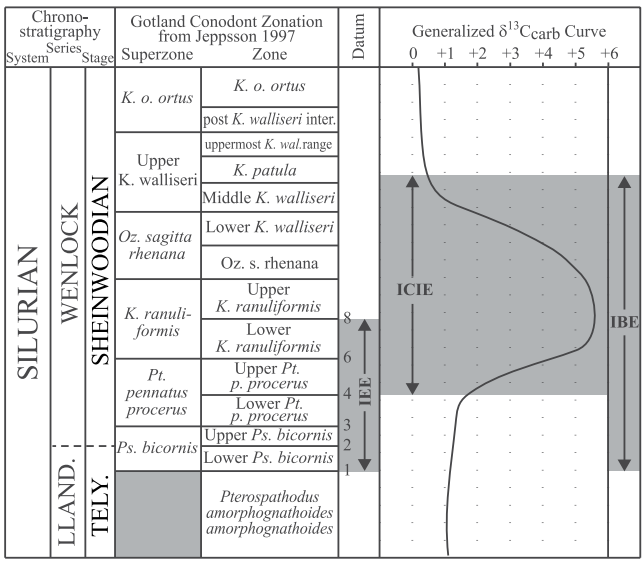

Figure 3. Conodont biozones, extinction datums, and the positive carbonate carbon isotope excursion during lower Sheinwoodian showing the relationships between the Ireviken Extinction Event (IEE), the Ireviken Carbonate Carbon Isotope Excursion (ICIE), and the Ireviken Biogeochemical Event (IBE). Conodont zones and extinction datums from Jeppsson (1997b). Ps. = Pseudooneotodus, p. = pennatus, K. = Kockelella, Oz. = Ozarkodina, s. = sagitta, o. = ortus. The term IBE is used to encompass all events in this interval from the onset of the extinction to the end of the carbon cycle perturbation and follows the use of Hartke et al. (2021).

began its initial inflection toward higher values at Datum 4 and elevated values persist until the middle part of the Sheinwoodian Stage (Cramer & Jarvis, 2020; Cramer et al., 2010a; Melchin et al., 2020; Munnecke et al., 2003).

New data from Hartke et al. (2021) revealed previously unknown details in the carbon isotope excursion as a result of high-resolution sampling of the Altajme core and demonstrated asynchronous behavior between the $\delta^{13}C_{carb}$ and $\delta^{13}C_{org}$ signals during the onset of the IEE and before the positive excursion in $\delta^{13}C_{carb}$, where a transient negative excursion in $\delta^{13}C_{org}$ was recorded prior to the traditional positive ICIE which is defined by the onset of the positive carbonate carbon isotope excursion at Datum 4 (Figure 3).

1.2. Microbial Sulfate Reduction

The $\delta^{34}S$ sulfur isotopic system is a measure of the relative proportion of $^{34}S/^{32}S$ that varies through time in the global ocean and is affected by sulfide and sulfate input and removal to and from the oceans by riverine input, volcanism, hydrothermal activity, and deposition of evaporites and sulfide minerals (e.g., Bottrell & Newton, 2006). Out of all these processes, the Microbial Sulfate Reduction (MSR) pathway produces the largest fractionation (up to −70‰, Canfield et al., 2010; Paytan et al., 2020; Sim et al., 2011) on the marine sulfate reservoir through the dissimilatory reduction of sulfate to sulfide and is the dominant control on the $\delta^{34}S$ value in the rock record. MSR is an anaerobic process that can occur through a variety of metabolic pathways that utilize sulfate and organic carbon to produce energy. The most typical reaction pathways produce H_2S and HCO_3^- as byproducts through Equation 1:

$$SO_4^{2-} + 2CH_2O \rightarrow H_2S + 2HCO_3^- \quad (1)$$

This process typically imparts large fractionation on the marine sulfate reservoir by preferentially incorporating ^{32}S into the reduced H_2S product. This byproduct of MSR, when in the presence of reactive Fe (typically reduced Fe^{2+}), will promote pyrite (FeS_2) burial in reduced settings and incorporate the ^{32}S-enriched sulfur into these sedimentary sulfides. The process of sulfate reduction and sulfide deposition via MSR requires that sulfate is available as an oxidant, organic matter is available for sulfate-reducing bacteria, and reactive Fe is present to react with H_2S. In the global ocean SO_4^{2-} and reactive Fe are typically non-limiting, and it is the abundance of organic carbon and the anoxic environments required that limit MSR (Paytan et al., 2020). This process of sulfate reduction and iron sulfide precipitation are limited to environments that lack oxygen and contain free hydrogen sulfide, that is, euxinic environments. The removal of ^{32}S from the marine sulfate reservoir will therefore leave the remaining pool of sulfur in the global oceans comparatively enriched in ^{34}S and produce a positive $\delta^{34}S$ signal during intervals of enhanced pyrite burial due to expanded euxinic marine environments. The sulfur isotope system can be recorded by sulfates such as barite or CAS ($\delta^{34}S_{CAS}$) or by sedimentary sulfides, such as pyrite ($\delta^{34}S_{py}$). These two signals are complementary and changes in the sulfur isotopic composition of the local water mass and/or pore waters are recorded by $\delta^{34}S_{py}$ data and the typically more global record of changes to the marine sulfate reservoir are recorded by $\delta^{34}S_{CAS}$. Furthermore, the sulfur isotopic composition of CAS in modern biogenic carbonates and bulk micrites robustly matches that of contemporaneous seawater within ≤1‰ (Burdett et al., 1989; Kamschulte et al., 2001; Kampschulte & Strauss, 2004; Lyons et al., 2004; Strauss, 1999).

A variety of local and/or diagenetic processes can impart fractionations on $\delta^{34}S$ records preserved in marine strata including the weathering of evaporite lithologies (Wortmann & Paytan, 2012), platform-scale dolomitization processes (e.g., Richardson et al., 2021), or closed system behavior (Present et al., 2015, 2019; Richardson et al., 2019; Rose et al., 2019) resulting from changes in local depositional environment or eustatic sea level fluctuations. Given these caveats, it is important to operate from first principles when interpreting $\delta^{34}S$ records and great care must be taken to compare all available sedimentological, geochemical, and biological records available to identify the most parsimonious interpretation of any given record.

Sedimentary sulfates and sulfides can both record secular changes in $\delta^{34}S$ but these minerals are typically generated in different environments, even when recorded from the same strata. In the case of CAS, the sulfate is incorporated as a trace component into carbonate minerals during their formation. Carbonate production typically occurs in shallower waters within the photic zone and the incorporation of sulfate carries little fractionation (Burdett et al., 1989; Kampschulte et al., 2001; Kampschulte & Strauss, 2004; Lyons et al., 2004; Strauss, 1999), which makes $\delta^{34}S_{CAS}$ an attractive archive of global changes in isotopic composition of the marine sulfate reservoir. However, as more data become available from multiple areas for a single event, it is becoming increasingly clear that the $\delta^{34}S_{CAS}$ does not always preserve a straightforward global record of synchronous change in all settings (e.g., see Present et al., 2019; Richardson et al., 2021). Pyrite is typically formed through biologically mediated pathways (such as MSR) within sedimentary pore waters or deep euxinic portions of a water column. The $\delta^{34}S_{py}$ record is therefore affected by local sedimentary and environmental conditions such as temperature, porosity, pore water chemistry, and diffusion rates, and is used as a proxy for the local expansion of reduced environments. In both cases ($\delta^{34}S_{CAS}$ and $\delta^{34}S_{py}$), an expansion of reducing environments that promoted burial of reduced carbon and sulfur, as organic carbon and pyrite, respectively, would generate a positive $\delta^{34}S$ excursion as progressively more ^{32}S was removed from either the global ($\delta^{34}S_{CAS}$) or local ($\delta^{34}S_{py}$) sulfate reservoir.

2. Materials and Methods

2.1. Sample Preparation

The Altajme core was drilled in 2015 and half of the entire core resides at the Department of Geology, Lund University, and the other half was used in this study. The sampled half of the core at the University of Iowa has been registered with the System for Earth Sample Registration with the unique International Geosample Registry Number IEBDC0001. For this project, 72 samples were collected spanning from the Telychian Stage of the Llandovery Series through much of the Sheinwoodian Stage of the Wenlock Series over an interval that includes the entire Ireviken carbonate carbon isotope excursion. A roughly 2–3 cm thick interval of 7.5 cm diameter core was taken at regular intervals with some variation to avoid any heterogeneous surfaces, such as hardgrounds, and the outer edge of the core was removed prior to sample processing. Samples were prepared using a SPEX 8510 Shatterbox and ∼60 g was powdered/homogenized in alumina ceramic containers for CAS and pyrite sulfur isotope analyses. The powdered samples were processed and analyzed at Florida State University and the National High Magnetic Field Laboratory using the procedures outlined below.

2.2. Geochemical Analyses

Using a similar procedure outlined by Wotte et al. (2012), CAS was extracted from sample powders by weighing 60–80 g of sample and then rinsing and agitating them for 12 hr with 500 mL of 10% NaCl. The salt rinse was repeated three times, and then rinsed and agitated in ultrapure water three times for ∼12 hr to remove water soluble sulfate. To dissolve all carbonate minerals and liberate the incorporated sulfate from the matrix, samples were acidified using 6M HCl for ≤2 hr. This step was done with short duration to minimize oxidation of sedimentary pyrite. The acidified solution was then separated from the insoluble residues via centrifugation and the residues were used for pyrite sulfur extraction. Sample solutions were filtered and then buffered to a pH ∼4. Excess $BaCl_2$ solution was added to quantitatively precipitate $BaSO_4$. The $BaSO_4$ precipitate was rinsed with ultrapure water and centrifuged multiple times to remove any potential chlorine compounds and dried overnight at 75°C prior to isotopic analysis. From the remaining acid-insoluble residues, pyrite sulfur was extracted using a mixture of ∼70 ml of 12M HCl and ∼30 ml of 1.0M chromium chloride ($CrCl_2 \bullet 6H_2O$) in an N_2-purged extraction flask. Evolved H_2S gas was passed through a buffered solution (0.1 M sodium citrate) and then into a 0.1M $AgNO_3$ solution to precipitate Ag_2S (Brüchert & Pratt, 1996). The Ag_2S precipitate was then filtered, rinsed, dried, and weighed for concentration and isotopic analysis.

First, the homogenized $BaSO_4$ and Ag_2S powders were placed into tin capsules with excess V_2O_5. The $\delta^{34}S$ content was then analyzed by the SO_2 method using a Thermo EA-Isolink coupled to a Thermo Delta V Plus isotope ratio mass spectrometer via a Conflo IV split interface. Isotope ratios are reported in per mil (‰) and use delta notation relative to Vienna Canyon Diablo Troilite (V-CDT). Calibration via the SO_2 method was completed based on internal laboratory standards EMR-CP (+0.9‰), PQM2 (−16‰), ERE (−4.7‰), PQB-D (+40.5‰), and SWP (+20.3‰) that have been calibrated relative to international standards NBS-127–$BaSO_4$

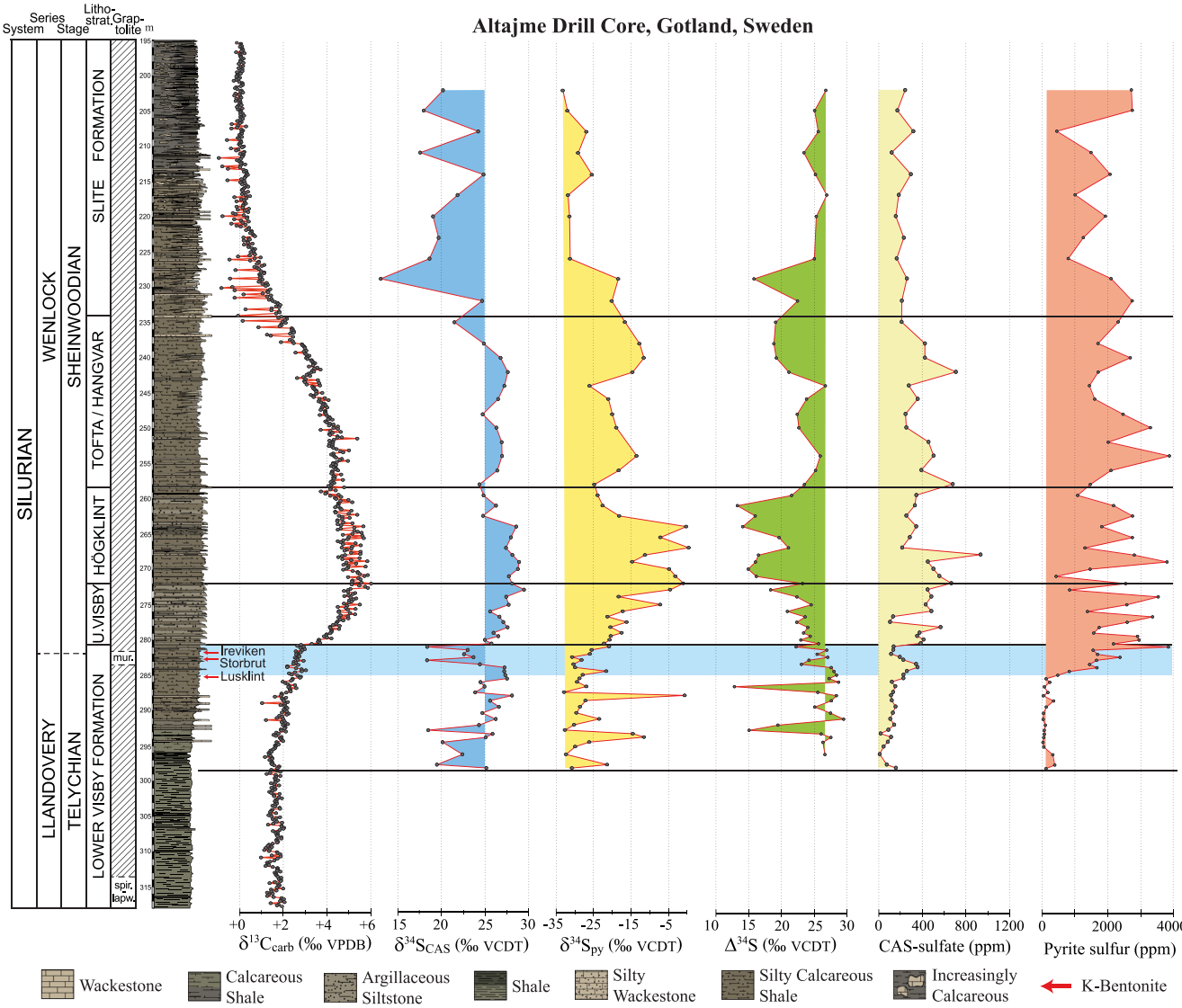

Figure 4. New sulfur data from the Altajme core shown against the stratigraphic column and carbonate carbon isotope data from Hartke et al. (2021). Blue box corresponds to the interval from the onset of the Ireviken Extinction Event (see Hartke et al., 2021) to the onset of the Ireviken Biogeochemical Event. $\delta^{34}S_{py}$, Carbonate Associated Sulfate (CAS) and pyrite concentrations all show a significant increase starting within this interval. (Inflection for shading at an arbitrary position.)

($\delta^{34}S$, +20.3‰) and IAEA S-1–Ag_2S ($\delta^{34}S$, −0.30‰). The analytical precision, based on long-term, replicate analysis of lab standards calibrated to IAEA standards at the National High Magnetic Field Laboratory at Florida State University (NHMFL-FSU), is ±0.2‰ or better (1σ).

3. Data

All sulfur isotope and concentration data produced in this study (Stolfus et al., 2022) are shown alongside the carbon isotope data produced in Hartke et al. (2021). Their data are crucial to show the fine-scale temporal relationships between the carbon isotope system and the sulfur data presented here. The blue box shown in Figure 4, starting at approximately 285 m, occurs near the beginning of the IEE and marks the onset of the interval that Hartke et al. (2021) identified as significant due to an apparent decoupling in the carbonate isotopic record where a short-lived negative excursion in $\delta^{13}C_{org}$ precedes the onset of the positive excursion in $\delta^{13}C_{carb}$ (beginning at the top of the blue box) traditionally referred to as the ICIE.

The $\delta^{34}S_{CAS}$ signal from the Altajme core preserves a lower amplitude positive isotope excursion than what was recovered from the outcrop belt on Gotland by Rose et al. (2019) that is broadly correlative with the Ireviken

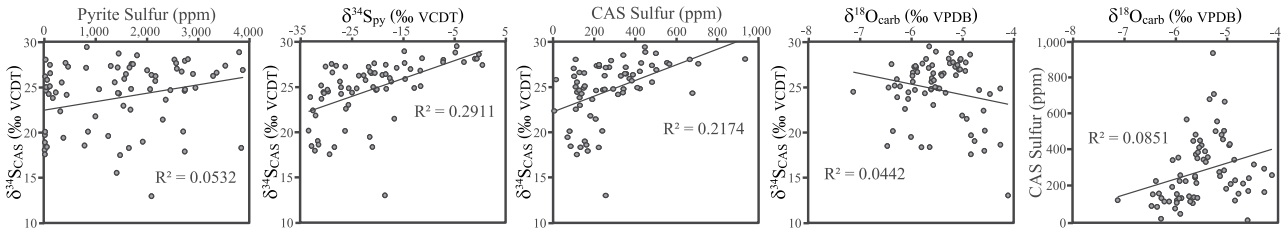

Figure 5. $\delta^{34}S_{CAS}$ versus pyrite sulfur concentrations, $\delta^{34}S_{CAS}$ versus $\delta^{34}S_{py}$, $\delta^{34}S_{CAS}$ versus $\delta^{18}O_{carb}$, and CAS sulfur concentrations versus $\delta^{18}O_{carb}$ in the Altajme core. $\delta^{18}O$ data from Hartke et al. (2021).

positive carbon isotope excursion. Before the ICIE the $\delta^{34}S_{CAS}$ values are highly variable with a range of 18.3‰ to 28.1‰ and transition to more consistently higher values during the ICIE. However, beginning at 280.6 m values appear to show a weak positive excursion where values begin at 25.7‰ and reach their highest value of 29.4‰ at 273 m. $\delta^{34}S_{CAS}$ remains above +25‰ until 238 m where they decline during the descending limb of the ICIE. Above this position, $\delta^{34}S_{CAS}$ reaches the lowest values of 13.0‰ at 229 m.

CAS concentration broadly mirror the $\delta^{34}S_{CAS}$ signal with typically higher values during the ICIE interval (~280–225 m) and the highest concentrations occur during the same interval that has the highest carbonate carbon isotope values. The initial increase in CAS concentrations begins at 286 m, below the onset of the positive ICIE and is nearly coincident with the base of the blue box highlighted in Figure 4. This initiation is therefore nearly precisely coincident with the onset of the extinction interval of the IEE marked by Datum 1 (Figure 3). From this point upwards, CAS concentrations gradually increase and reach peak values of 930 ppm at 268 m. Values remain generally above 200 ppm during the remainder of the ICIE interval and return to a new baseline of approximately 200 ppm following the end of the ICIE.

Below 282 m $\delta^{34}S_{py}$ values are typically between −32.0 and −25.0‰ with a few outliers that are single or double data points reaching highs of −0.62‰. At 282 m a positive $\delta^{34}S_{py}$ excursion begins and trends upwards until about 265 m where multiple samples record values above −5.0‰. The onset of the positive $\delta^{34}S_{py}$ excursion begins prior to the onset of the ICIE within the blue box shown in Figure 4. $\delta^{34}S_{py}$ values remain elevated typically above −25.0‰ to 226 m where there is a decrease to −31.5‰ roughly coincident with the end of the ICIE.

Pyrite sulfur concentration are low and remarkably stable (typically <<400 ppm) prior to the IBE up until approximately 285 m where an increase begins at roughly the same level as the onset of IBE (base of blue box in Figure 4). Pyrite sulfur concentrations increase rapidly during the onset of the extinction interval to nearly 4,000 ppm at 280.5 m (top of the blue box in Figure 4) and the onset of the ICIE. Pyrite sulfur concentrations remain high throughout the remainder of the studied core interval but with considerable variability and values ranging from a low of 410 ppm at 271 m to a peak value of ~3,800 ppm at 253.9 m.

4. Results

4.1. Data Reliability and Comparison With Other Silurian $\delta^{34}S$ Records

Carbonate recrystallization during diagenetic alteration can modify the original geochemical signals of carbon, oxygen, and sulfur through a variety of processes including water-rock interactions, remineralization of organic matter, thermal maturation, or the oxidation and remineralization of reduced species (organic carbon or pyrite). The lack of systematic covariation in $\delta^{18}O_{carb}$ with $\delta^{13}C_{carb}$ in the Altajme core (Hartke et al., 2021) demonstrate that the strata have not experienced any significant diagenetic resetting of the original isotopic signatures due to meteoric or pore-fluid diagenesis (Ahm et al., 2018; Algeo et al., 1992; Banner & Hanson, 1990; Swart & Oehlert, 2018). Similarly, the lack of covariation in $\delta^{13}C_{org}$ with TOC% (Total organic carbon [TOC]), and the low color alteration index (CAI) of conodonts from Gotland and the Altajme core (CAI ≤ 1), indicate a maximum burial temperature of no higher than 80°C (Epstein et al., 1977) and demonstrate a lack of diagenetic alteration through thermal maturation or oxidation of volatile organic compounds. Cross plots of $\delta^{34}S_{CAS}$, (pyrite sulfur), $\delta^{34}S_{py}$, (CAS), and $\delta^{18}O$ show the same lack of significant diagenetic co-variation (Figure 5).

The only relationship in Figure 5 with even a weak correlation is between the $\delta^{34}S_{py}$ and $\delta^{34}S_{CAS}$ record, which has an R^2 value of 0.29. Given that both datasets are recording the sulfur isotope system response during the IBE, it

should be expected that there is at least some relationship. If diagenetic recrystallization were imposing a significant resetting of original marine values with meteoric and/or otherwise secondary values, we would expect to see a linear or asymptotic relationship between several of these values, particularly a relationship with $\delta^{18}O$ (Ahm et al., 2018; Swart & Oehlert, 2018). Collectively however, these relationships (Figure 5) demonstrate that there was no significant wholesale resetting of primary geochemical values in the Altajme core, and that the system was predominantly sediment buffered during its geological history.

Authigenic barite and well-preserved brachiopod calcite are ideal materials to recover original marine $\delta^{34}S_{sulfate}$ values due to the low "noise" and resistance to diagenetic resetting of the original marine signal (e.g., Present et al., 2015). Unfortunately, neither material is suitable for high-resolution studies that require chronostratigraphically dense sample spacing. Bulk CAS of carbonates, which are available for high-resolution chemostratigraphy, has been shown to faithfully record secular changes in $\delta^{34}S_{sulfate}$ when compared directly to barite and foraminifera during the Cenozoic (Toyama et al., 2020; Yao et al., 2020). However, fine-grained carbonates have also been shown to contain a mixture of original marine sulfate as well as secondary cements that carry an MSR-derived $\delta^{34}S_{sulfate}$ signal (Edwards et al., 2017; Present et al., 2019). In these lithologies, the preferential removal of ^{32}S by MSR leaves a residual sulfate pool enriched in ^{34}S that can be incorporated into secondary mineralization and result in abnormally positive $\delta^{34}S_{CAS}$ values compared to the contemporaneous global $\delta^{34}S_{sulfate}$ values. This mechanism is unlikely to have affected the $\delta^{34}S_{CAS}$ record in the Altajme core, despite the overall fine-grained texture, because the $\delta^{34}S_{CAS}$ signal recovered appears to be attenuated compared to other global records (Figure 6), including those from Gotland and elsewhere in the Baltic Basin (Richardson et al., 2019; Rose et al., 2019; Young et al., 2020).

Sedimentary pyrite oxidation and organic sulfur oxidation both have the ability to alter original geochemical signals and specifically the $\delta^{34}S_{CAS}$ record. Pyrite is a reactivate mineral and can oxidize during diagenesis or during chemical extraction of CAS when exposed to oxidizing and/or highly acidic conditions (Wotte et al., 2012). Similarly, oxidation of organic sulfur compounds can occur during the extraction process (e.g., Marenco et al., 2008), and this would be most significant during intervals of elevated TOC contents in our core. This alteration, from either diagenesis or oxidation during sample acidification, will result in the increased incorporation of ^{32}S into the dissolved sulfate fraction and can result in an artificial decrease in $\delta^{34}S_{CAS}$ values recorded. In the $\delta^{34}S_{CAS}$ record of the Altajme core, there appears to be an attenuated positive isotopic excursion compared to other $\delta^{34}S_{CAS}$ records (Figure 6) through the IBE (Richardson et al., 2019; Rose et al., 2019; Young et al., 2019). The most obvious explanation for this attenuation of the $\delta^{34}S_{CAS}$ record from the Altajme core would be sedimentary pyrite and/or organic sulfur contamination via oxidation during processing given the high amount of pyrite in these samples, the elevated TOC values during the IBE, and no other obvious indications of diagenetic alteration. Such alteration of the original $\delta^{34}S_{CAS}$ signal by the products of pyrite oxidation would be expected to show a correlation between pyrite sulfur concentration and $\delta^{34}S_{CAS}$ isotopes, but in the Altajme core (Figure 5) we see no significant correlation. The lack of significant correlation suggests, again, there was no wholesale resetting of $\delta^{34}S_{CAS}$ values, however, the demonstrably attenuated trends compared to $\delta^{34}S_{CAS}$ values from Gotland (e.g., Rose et al., 2019, which is <60 km away), elsewhere in the Baltic Basin (Richardson et al., 2019), and from distant sections in other basins (Young et al., 2019), combined with the high pyrite concentration of this interval in the Altajme core, demonstrate that the potential impact of sedimentary pyrite oxidation on our $\delta^{34}S_{CAS}$ data cannot be ruled out. Another equally parsimonious explanation for the diminished $\delta^{34}S_{CAS}$ values in our data compared with those from Gotland produced by Rose et al. (2019) is the potential oxidation of organic sulfur compounds during the sample extraction steps. Organic sulfur compounds are another important, but often understudied, potential sink of reduced sulfur in marine sediments (e.g., Raven et al., 2019). TOC contents clearly increases during the IBE (see Figure 7 below and Hartke et al., 2021) and the most significant impacts of attenuation of the $\delta^{34}S_{CAS}$ signal would have been primarily limited to this interval.

What is most interesting to note in the compilation of sulfur isotope data from Figure 6 is the range of variability in data from section to section in both the CAS and pyrite records. For example, the data from Gotland (Rose et al., 2019), Nevada (Young et al., 2019), and Estonia (Richardson et al., 2019) all show a clear increase in $\delta^{34}S_{CAS}$ during the onset of the IBE with higher values during the earliest Sheinwoodian compared to the latest Telychian. The data from Tennessee (Young et al., 2019) and Estonia (Richardson et al., 2021) do not record sufficient values from prior to the IBE to identify what baseline values would have been prior to the IBE, but both show a decrease in $\delta^{34}S_{CAS}$ at the end of the IBE interval. Taken together, the $\delta^{34}S_{CAS}$ data compiled in Figure 6

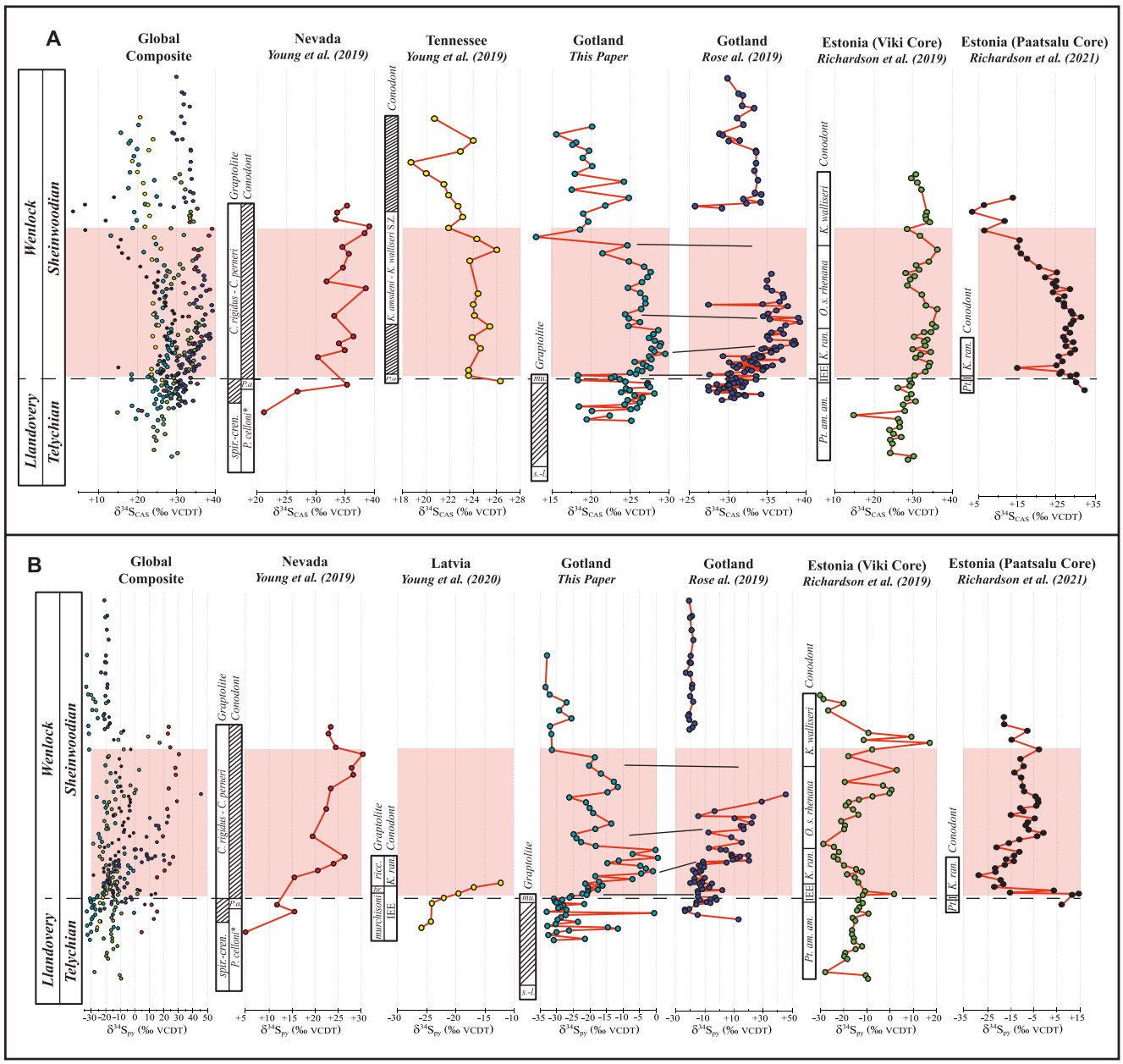

Figure 6. (a) Comparison of $\delta^{34}S_{CAS}$ values from Nevada and Tennessee (Young et al., 2019), Estonia (Richardson et al., 2019), the outcrop belt of northwest Gotland (Rose et al., 2019), and the new data from the Altajme core. (b) Comparison of $\delta\ ^{34}S_{py}$ values from Nevada (Young et al., 2019), Latvia (Young et al., 2020), Estonia (Richardson et al., 2019, 2021), the outcrop belt of northwest Gotland (Rose et al., 2019), and the new data from the Altajme core. Pink box highlights the interval of the ICIE. Dashed line shows the position of the Llandovery-Wenlock boundary in each section. Solid lines between the Altajme core data and the outcrop data of Rose et al. (2019) show formation boundaries as correlation Note: Most of the Telychian samples from the Paatsalu core shown in Richardson et al. (2021) come from the Pterospathodus amorphognathoides lithuanicus zone or older strata and are below the interval shown here.

clearly demonstrate an increase in the $\delta^{34}S_{CAS}$ record is a common feature of most of the data available in the literature (Gotland, Estonia-Viki, and Nevada).

What is clear from the data compiled in Figure 6 is that all records recovered that include sufficient data from prior to the IBE show some positive excursion in $\delta^{34}S_{CAS}$ values coincident with the positive increase in $\delta^{13}C$ during the ICIE that is most parsimoniously explained by a fundamental change in the seawater $\delta^{34}S_{sulfate}$ values during this global event. It is also clear that the absolute values of $\delta^{34}S_{CAS}$ vary significantly from section to section even though the geometry of changes (increase or decrease) seems to be consistent. The differences

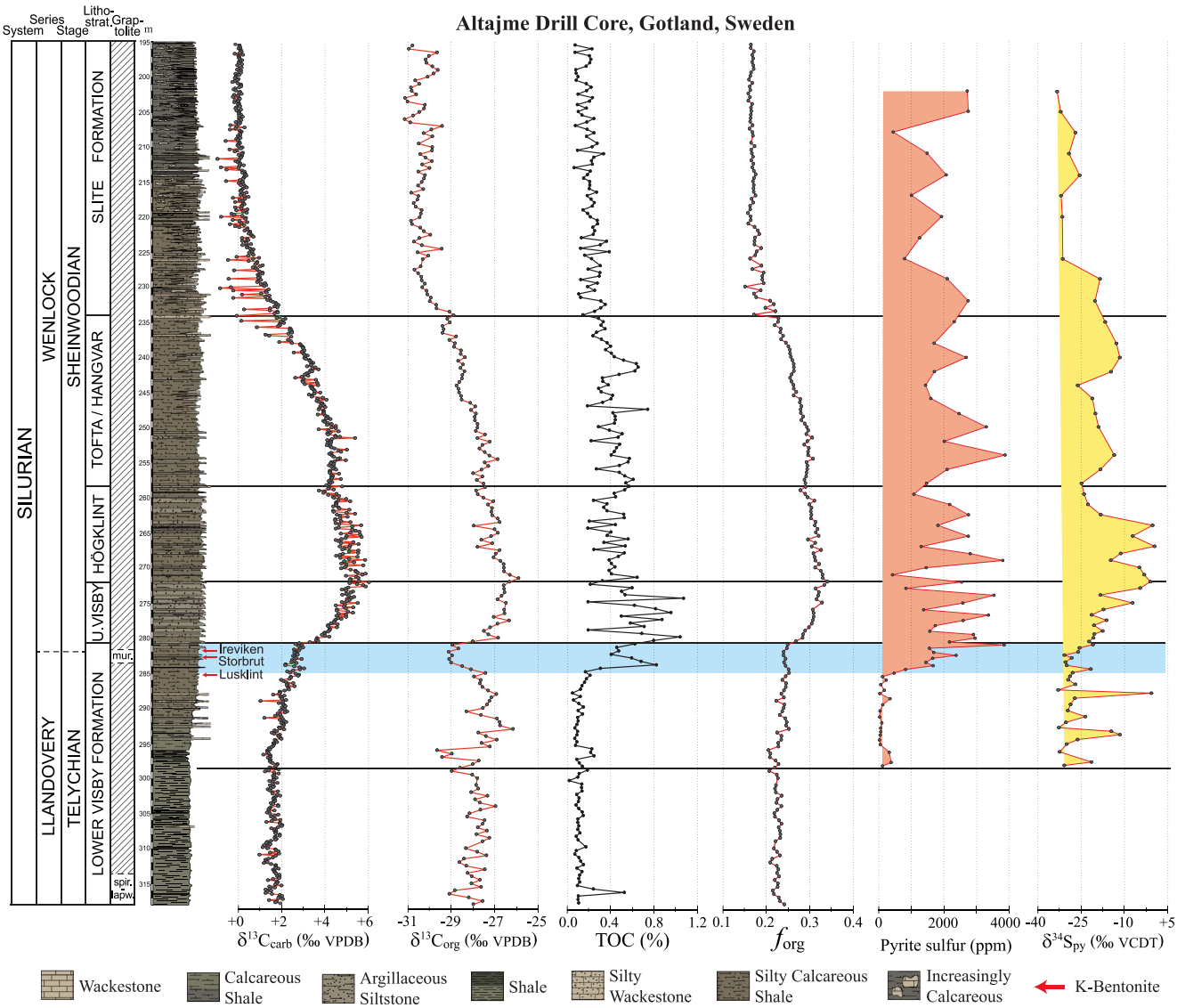

Figure 7. Pyrite sulfur and $\delta^{34}S_{py}$ from this study combined with carbon isotope, total organic carbon (TOC), and interpreted fraction of organic carbon burial (f_{org}) from Hartke et al. (2021). The TOC content and pyrite concentrations increase synchronously illustrating their common driver whereas the $\delta^{13}C_{carb}$, f_{org}, and $\delta^{34}S_{py}$ signals similarly change in unison owing to their common drivers.

in $\delta^{34}S_{CAS}$ excursion magnitude and absolute baseline values are best explained by a spatially heterogeneous sulfate reservoir in the early Silurian oceans and concentrations substantially lower than the modern ocean (Gill et al., 2007; Lowenstein et al., 2003; Yao et al., 2019; Young et al., 2019). Furthermore, all of the records with the exception of Estonia also show a concomitant increase in $\delta^{34}S_{py}$ values illustrating the local changes in marine sulfur cycling that would be mandatory to generate a global shift in the marine $\delta^{34}S_{sulfate}$ signal recorded by the positive excursion in $\delta^{34}S_{CAS}$. The major advance of the high-resolution data presented here is the demonstration of the timing of the changes in local marine sulfur cycling in the Altajme core, deeper shelf setting of the Baltic Basin, with respect to the global marine carbon isotope signal.

4.2. Local Redox and the Altajme Core

Within the Altajme core, we see an increase in pyrite burial and a positive excursion in $\delta^{34}S_{py}$ that broadly corresponds with the Ireviken positive carbon isotope excursion (ICIE), but in detail the onset of pyrite burial and the $\delta^{34}S_{py}$ excursion both slightly precede the onset of the ICIE within the blue box in Figure 7. The initiation of

increased pyrite burial is virtually coincident with the increase in TOC occurring at the onset of the IEE (bottom of blue box in Figure 7). This increase in organic carbon would have provided the organic carbon substrate for MSR that is often the dominant control on the MSR pathway and eventually leads to increased pyrite formation and burial given sufficient Fe in the system. The evidence of increased MSR (pyrite concentrations and $\delta^{34}S_{py}$) and coincident enhanced organic carbon burial (TOC) both indicate an increase in local anoxic conditions at the onset of the IBE and the combined records of $\delta^{13}C_{carb}$, $\delta^{13}C_{org}$, TOC, sedimentary pyrite, and $\delta^{34}S_{py}$ begin to demonstrate how the IBE unfolded at this locale. The initial expansion of reducing bottom waters in this area of the Baltic Basin, among many other basins, increased organic carbon burial, which preferentially removed ^{12}C from the oceanic reservoir and initiated a positive carbon isotope excursion. Creation of pyrite via the MSR pathway was enhanced by this expansion of reducing environments, in which the H_2S byproduct bonded with Fe to form pyrite, and began to deplete the sulfate reservoir of ^{32}S and resulted in the positive $\delta^{34}S_{py}$ excursion recorded in the Altajme core. Ultimately, the removal of reduced carbon and sulfur (^{12}C and ^{32}S), as organic carbon and pyrite, were promoted by the deoxygenation event that must have been initiated at the onset of the IBE (blue box in Figure 7).

The expansion of reducing environments onto the continental shelves, and in this case within the Baltic Basin, during the IBE demonstrates a critical lithological juxtaposition discussed previously by Cramer and Saltzman (2005, 2007), and again by Young et al. (2019). Namely, this expansion of reducing environments was taking place simultaneously with the expansion of carbonate reef environments in shallower up-ramp settings (Figure 8). The interval of the IBE is well known for its expanding reef environments and ubiquitous carbonate platforms (e.g., Brunton et al., 1998; Cramer & Saltzman, 2007; Munnecke et al., 2010, 2003) and this feature is echoed in the deeper off-ramp setting of the Altajme core. The lithology of the IBE interval preserved in the Altajme core is progressively more calcareous through the early Sheinwoodian with almost exclusively <30% carbonate prior to the IBE and almost exclusively >30% carbonate during and after the IBE, with some intervals of the Upper Visby, Högklint, and Tofta formations having >60% carbonate as material from up ramp environments was exported farther out into the basin and across the location of the Altajme core (Hartke et al., 2021). The interval of the IBE in the Altajme core is comprehensively bioturbated and lacks fine-scale laminations suggesting that the immediately overlying water column contained at least some available oxygen. Therefore, the position of the Altajme core must have been sufficiently up ramp to be outside of any potential mid-water oxygen minimum zone yet was clearly basinward of the Högklint and Tofta reef complexes that were forming during the IBE.

It is important to point out that enhanced MSR and pyrite burial can increase the alkalinity and [HCO_3^-] in surrounding water masses, which would favor carbonate precipitation in general. Hyper-calcification is a known feature of the earliest Sheinwoodian (Sequence V of Cramer et al., 2010b, earliest peak values in $\delta^{13}C_{carb}$, Högklint Formation herein) and is seen in both the Högklint Formation in outcrop on Gotland (e.g., Brunton et al., 1998; Munnecke et al., 2010) as well as the Bisher Formation in the Appalachian Basin (Oborny et al., 2020). As pointed out by Munnecke et al. (2010), microbial carbonates, and calcifying cyanobacteria in particular, are an abundant component of carbonate deposition in many locations during this interval. Given that most calcifying cyanobacteria produce calcium carbonate outside of their cells and in direct contact with seawater, their rate of calcification will be greatly impacted by any potential change in alkalinity induced by MSR and increase pyrite burial, and this coincidence during the early part of the IBE is additional supporting evidence of the interpretation presented here.

4.3. Reducing Environments and Ireviken Oceanic Anoxic Event

A scenario for the expression of the IBE in the Baltic Basin and the Altajme core are shown in Figure 8. A variety of potential triggers for the onset of the IBE have been proposed (e.g., Cramer & Saltzman, 2007; Emsbo, 2017; Munnecke et al., 2010; Vandenbroucke et al., 2015) and Hartke et al. (2021) recently framed the series of events during the onset of the IBE within a broader discussion of similarities to Mesozoic Oceanic Anoxic Events. In the case of the Altajme core presented here, it is clear that an initial increase in locally reducing environments favored preservation of ^{12}C and ^{32}S during the initiation of the IEE immediately prior to the onset of the ICIE. Given that the $\delta^{13}C_{carb}$ record typically responds to changes in the isotopic value of the global dissolved inorganic carbon (DIC) reservoir (e.g., Hayes et al., 1999), this temporal offset between TOC and pyrite burial versus the $\delta^{13}C$ record is demonstration that (a) the $\delta^{13}C_{carb}$ record in the Altajme core is not exclusively the result of local organic carbon burial (otherwise they would be synchronous), and (b) that the enhanced burial of TOC and

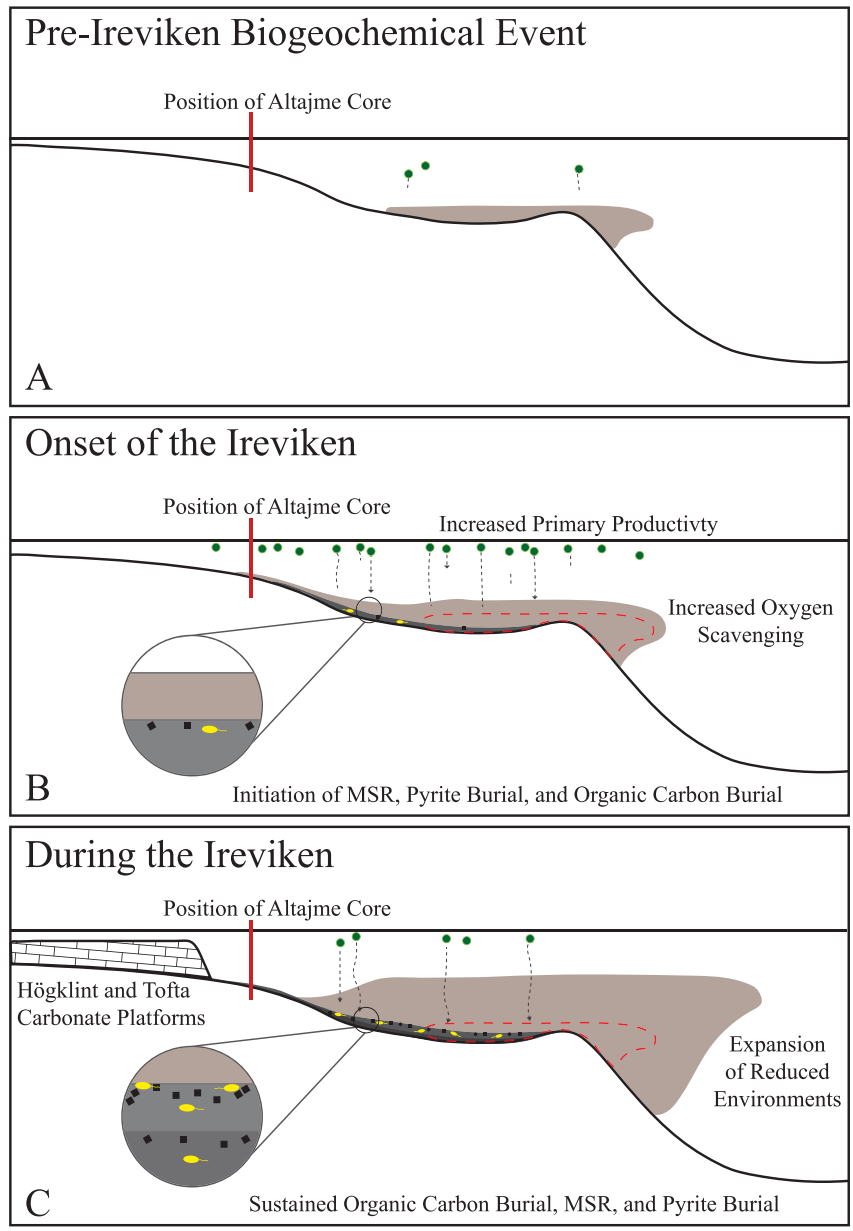

Figure 8. Schematic reconstruction of the expansion of reduced environments in the study area during the Ireviken Biogeochemical Event (IBE). (a) Shelf environment prior to the IBE. Small area of reduced environments (shaded tan area) that produce organic carbon rich sediments in distal settings. (b) Increased nutrient availability fuels primary productivity (green dots) and results in oxygen scavenging by decaying organic matter and reduced metals. Deoxygenation initiates microbial sulfate reduction (MSR; yellow ovals), pyrite burial (black squares), and deposition of organic carbon rich sediments (shaded gray area). (c) Expansion of reducing environments leads to sustained organic carbon burial, MSR, and pyrite burial further into shelf/slope settings and coincides with maximum carbonate platform production (modified from Cramer and Saltzman (2007) and Young et al. (2019)).

pyrite were the local expression of a wider regional-to-global event that favored preservation of ^{12}C and ^{32}S on a scale significant enough to drive global positive excursions in $\delta^{13}C$ and $\delta^{34}S_{CAS}$ (Figure 6). The duration and timing of the geochemical changes during the onset of the IBE, and illustrated in the Altajme core are important to note. The entire IBE is somewhere approximating 1–1.5 Myr in duration (Cramer & Jarvis., 2020; McAdams et al., 2019; Melchin et al., 2020), and the interval of the extinction event and onset of the geochemical perturbations in carbon and sulfur are likely in the order of less than 200 kyr (e.g., McAdams et al., 2019). Therefore, the short duration in the offset between the carbon isotope and the sulfur isotope records shown in the Altajme

core provide important data in the evaluation of the potential response time of the marine sulfur cycle, and by implication the size of the marine sulfate reservoir at the onset of the IBE in the early Silurian (e.g., 5 mM sulfate reservoir; Young et al., 2019). As previously mentioned, the local expansion of reduced settings is indicated by the onset of the pyrite sulfur ppm and TOC % increase prior to the $\delta^{13}C_{carb}$ excursion at the beginning of the blue box in Figure 7. At precisely the same time, there is a negative excursion in $\delta^{13}C_{org}$ and this is likely due to an increase in the proportion of chemosymbiotic organic matter which has a lower $\delta^{13}C$ value and a more in depth discussion of this can be found in Hartke et al. (2021).

Whatever event may have initiated the expansion of reducing environments, and ultimately the IBE, the precise temporal relationship between expanding reducing environments (Figure 6), enhanced organic carbon and pyrite burial (Figure 7), a biotic crisis, and a major perturbation to the global carbon cycle during the IBE are all beginning to demonstrate that this was clearly a global event that involved fundamental changes in both the marine redox state as well as elemental and nutrient cycling within the oceans. That the extinction event (IEE) should precede the eventual consequence of enhanced organic carbon burial (ICIE) that resulted from expanding reducing environments should absolutely be expected as biology will immediately respond to any local oceanographic conditions, but globally dominated marine isotope records will require changes to the marine C reservoir (in this case the DIC pool) before the initial response will be apparent. What triggered the initial expansion of reducing environments remains unclear. However, whether the primary kill mechanism during the IEE was the reducing environments themselves, the remobilization of major and trace metals released from sedimentary iron-oxy-hydroxides as they were overrun by reducing conditions, the delivery of excess major- and trace metals from a non-marine source, or some other mechanism, it is clear that high-resolution investigations will be required to determine the ultimate cause-and-effect relationships within the ocean-atmosphere-biosphere system.

5. Conclusions

The $\delta^{34}S$ data from the Altajme core demonstrate several important features of redox change during the IBE. The increase in pyrite and organic burial that coincide with the ICIE are represented by coeval positive excursions in sedimentary pyrite, $\delta^{34}S_{py}$, $\delta^{13}C_{carb}$, $\delta^{13}C_{org}$, and TOC, and demonstrate that an expansion of reducing environments likely occurred at the onset of the IBE within the Baltic Basin. These data support the interpretation from Young et al. (2019) that the positive $\delta^{34}S_{CAS}$ excursion coincident with the IBE is globally indicative of increased pyrite burial. The expansive carbonate platforms of the Högklint and Tofta formations during this interval correspond to the peak values in the $\delta^{34}S_{py}$, $\delta^{13}C_{carb}$, $\delta^{13}C_{org}$ signals, which implies that the expansion of reduced environments corresponds with the increased carbonate production and expansion of a major carbonate reef platform in the Baltic Basin during the IBE. Furthermore, this study supports the interpretations of shoaling and expansion of reduced environments as a driver for increasing the burial fraction of organic carbon (f_{org}) that resulted in increased organic carbon burial and acted as the mechanism to produce the pronounced positive carbon isotope excursion (ICIE) during this interval.

Conflict of Interest

The authors declare no conflicts of interest relevant to this study.

Data Availability Statement

The samples analyzed in this study come from the Altajme Drill Core, IGSN: IEBDC0001. The new sulfur isotope data presented here are available for public access in the EarthChem Library at Stolfus et al. (2022).

Acknowledgments
This research was partially supported by grants from the U.S. National Science Foundation to B.D. Cramer (CAREER-1455030, EPSCOR-2119551). This work was completed as part of an M.S. Thesis in Geoscience (B.M. Stolfus) at the University of Iowa, Department of Earth and Environmental Sciences. S.A. Young and L.J. Allman would like to thank Joe Kerigan for his assistance with geochemical analyses. Sulfur isotopic analyses were performed at the National High Magnetic Field Laboratory in Tallahassee, Florida, which is supported by National Science Foundation Cooperative Agreement No. DMR-1644779 and by the State of Florida. This work was supported by the National Science Foundation Cooperative Agreement No. DMR-1157490 and the State of Florida.

References

Ahm, A.-S. C., Bjerrum, C. J., Blättler, C. L., Swart, P. K., & Higgins, J. A. (2018). Quantifying early marine diagenesis in shallow water carbonate sediments. *Geochimica et Cosmochimica Acta*, *236*, 140–159. https://doi.org/10.1016/j.gca.2018.02.042

Aldridge, R. J., Jeppsson, L., & Dorning, K. J. (1993). Early Silurian oceanic episodes and events. *Journal of the Geological Society*, *150*(3), 501–513. https://doi.org/10.1144/gsjgs.150.3.0501

Algeo, T. J., Wilkinson, B. H., & Lohmann, K. (1992). Meteoric-burial diagenesis of middle Pennsylvanian limestones in the Orogrande Basin, New Mexico: Water/rock interactions and basin geothermics. *Journal of Sedimentary Petrology*, *62*(4), 652–670.

Baarli, B. G., Johnson, M. E., & Antoshikina, A. I. (2003). Silurian stratigraphy and paleogeography of Baltica. In E. Landing & M. E. Johnson (Eds.), *Silurian lands and seas*, *New York State Museum Bulletin* (Vol. 49, pp. 3–34).

Banner, J. L., & Hanson, G. N. (1990). Calculation of simultaneous isotopic and trace element variations during water-rock interaction with applications to carbonate diagenesis. *Geochimica et Cosmochimica Acta*, *54*(11), 3123–3137. https://doi.org/10.1016/0016-7037(90)90128-8

Batchelor, R. A., & Jeppsson, L. (1994). Late Llandovery bentonites from Gotland, Sweden, as chronostratigraphic markers. *Journal of the Geological Society*, *151*(5), 741–746. https://doi.org/10.1144/gsjgs.151.5.0741

Berner, R. A. (2006). GEOCARBSULF: A combined model for Phanerozoic atmospheric O_2 and CO_2. *Geochimica et Cosmochimica Acta*, *70*(23), 5653–5664. https://doi.org/10.1016/j.gca.2005.11.032

Bickert, T., Pätzold, J., Samtleben, C., & Munnecke, A. (1997). Paleoenvironmental changes in the Silurian indicated by stable isotopes in brachiopod shells from Gotland, Sweden. *Geochimica et Cosmochimica Acta*, *61*(13), 2717–2730. https://doi.org/10.1016/S0016-7037(97)00136-1

Biebesheimer, E. J., Cramer, B. D., Calner, M., Barnett, B. A., Oborny, S. C., & Bancroft, A. M. (2021). Asynchronous $\delta^{13}C_{carb}$ and $\delta^{13}C_{org}$ records during the onset of the Mulde (Silurian) positive carbon isotope excursion from the Altajme core. *Gotland, Sweden: Chemical Geology*, *576*, 120256. https://doi.org/10.1016/j.chemgeo.2021.120256

Bottrell, S. H., & Newton, R. J. (2006). Reconstruction of changes in global sulfur cycling from marine sulfate isotopes. *Earth-Science Reviews*, *75*(1–4), 59–83. https://doi.org/10.1016/j.earscirev.2005.10.004

Brüchert, V., & Pratt, L. M. (1996). Contemporaneous early diagenetic formation of organic and inorganic sulfur in estuarine sediments from St Andrew Bay, Florida, USA. *Geochimica et Cosmochimica Acta*, *60*(13), 2325–2332. https://doi.org/10.1016/0016-7037(96)00087-7

Brunton, F. R., Smith, L., Dixon, O. A., Copper, P., Nestor, H., & Kershaw, S. (1998). Silurian reef episodes, changing seascapes, and paleobiogeography. *New York State Museum Bulletin*, *491*, 259–276.

Burdett, J. W., Arthur, M. A., & Richardson, M. (1989). A Neogene seawater sulfur isotope age curve from calcareous pelagic microfossils. *Earth and Planetary Science Letters*, *94*(3–4), 189–198. https://doi.org/10.1016/0012-821X(89)90138-6

Calner, M. (2008). Silurian global events at the tipping point of climate change. In M. T. Ashraf (Ed.), *Mass extinctions* (pp. 21–58). Springer-Verlag.

Calner, M., Jeppsson, L., & Erikson, M. E. (2005). The Baltic Basin and the Silurian strata of Gotland, Sweden. In M. E. Erikson, & M. Calner (Eds.), *The dynamic Silurian Earth: Subcommision on Silurian stratigraphy: Field guide and abstracts* (pp. 6–13).

Canfield, D. E., Farquhar, J., & Zerkle, A. L. (2010). High isotope fractionations during sulfate reduction in a low-sulfate euxinic ocean analog. *Geology*, *38*(5), 415–418. https://doi.org/10.1130/G30723.1

Cocks, L. R. M., & Torsvik, T. H. (2005). Baltica from the late Precambrian to mid-Paleozoic times: The gain and loss of a terrane's identity. *Earth-Science Reviews*, *72*(1–2), 39–66. https://doi.org/10.1016/j.earscirev.2005.04.001

Cooper, R. A., Sadler, P. M., Munnecke, A., & Crampton, J. S. (2014). Graptoloid evolutionary rates track Ordovician-Silurian climate change. *Geological Magazine*, *151*(2), 349–364. https://doi.org/10.1017/S0016756813000198

Cramer, B. D., Brett, C. E., Melchin, M. J., Männik, P., Kleffner, M. A., McLaughlin, P. I., et al. (2011). Revised correlation of Silurian Provincial Series of North America with global and regional chronostratigraphic units and $\delta^{13}C_{carb}$ chemostratigraphy. *Lethaia*, *44*(2), 185–202. https://doi.org/10.1111/j.1502-3931.2010.00234.x

Cramer, B. D., Condon, D. J., Söderlund, U., Marshall, C., Worton, G. J., Thomas, A. T., et al. (2012). U-Pb (zircon) age constraints on the timing and duration of Wenlock (Silurian) paleocommunity collapse and recovery during the "Big Crisis". *Geological Society of America Bulletin*, *124*(11–12), 1841–1857. https://doi.org/10.1130/B30642.1

Cramer, B. D., & Jarvis, I. (2020). Chapter 11: Carbon isotope stratigraphy. In F. M. Gradstein, J. G. Ogg, M. D. Schmitz, & G. M. Ogg (Eds.), *Geologic time scale 2020* (Vol. 1, pp. 309–343). Elsevier. https://doi.org/10.1016/B978-0-12-824360-2.00011-5

Cramer, B. D., Kleffner, M. A., Brett, C. E., McLaughlin, P. I., Jeppsson, L., Munnecke, A., et al. (2010b). Paleobiogeography, high-resolution stratigraphy, and the future of Paleozoic biostratigraphy; fine-scale diachroneity of the Wenlock (Silurian) conodont Kockelella Walliseri. *Paleogeography, Paleoclimatology, Paleoecology*, *294*(3–4), 232–241. https://doi.org/10.1016/j.palaeo.2010.01.002

Cramer, B. D., Loydell, D., Samtleben, C., Munnecke, A., Kaljo, D., Männik, P., et al. (2010a). Testing the limits of Paleozoic chronostratigraphic correlation via high-resolution (<500 k.y.) integrated conodont, graptolite, and carbon isotope ($\delta^{13}C_{carb}$) biochemostratigraphy across the Llandovery-Wenlock (Silurian) boundary: Is a unified Phanerozoic time scale achievable? *Geological Society of America Bulletin*, *122*(9–10), 1700–1716. https://doi.org/10.1130/B26602.1

Cramer, B. D., & Saltzman, M. R. (2005). Sequestration of ^{12}C in the deep ocean during the early Wenlock (Silurian) positive carbon isotope excursion. *Paleogeography, Paleoclimatology, Paleoecology*, *219*(3–4), 333–349. https://doi.org/10.1016/j.palaeo.2005.01.009

Cramer, B. D., & Saltzman, M. R. (2007). Early Silurian paired $\delta^{13}C_{carb}$ and $\delta^{13}C_{org}$ analyses from the Midcontinent of North America: Implications for paleoceanography and paleoclimate. *Paleogeography, Paleoclimatology, Paleoecology*, *256*(3–4), 195–203. https://doi.org/10.1016/j.palaeo.2007.02.032

Crampton, J. S., Cooper, R. A., Sadler, P. M., & Foote, M. (2016). Greenhouse-icehouse transition in the Late Ordovician marks a step change in extinction regime in the marine plankton. *Proceedings of the National Academy of Sciences of the United States of America*, *113*(6), 1498–1503. https://doi.org/10.1073/pnas.1519092113

Edwards, C. T., Saltzman, M. R., Royer, D. L., & Fike, D. A. (2017). Oxygenation as a driver of the Great Ordovician Biodiversification Event. *Nature Geoscience*, *10*(12), 925–929. https://doi.org/10.1038/s41561-017-0006-3

Emsbo, P. (2017). Sedex brine expulsions to Paleozoic basins may have changed global marine $^{87}Sr/^{86}Sr$ values, triggered anoxia, and initiated mass extinctions. *Ore Geology Reviews*, *86*, 474–486. https://doi.org/10.1016/j.oregeorev.2017.02.031

Epstein, A. G., Epstein, J. B., & Harris, L. D. (1977). *Conodont color alteration—An index to organic metamorphism* (Vol. 995, p. 27). United States Geological Survey Professional Paper.

Gelsthorpe, D. N. (2004). Microplankton changes through the early Silurian Ireviken extinction event on Gotland, Sweden. *Review of Paleobotany and Palynology*, *130*, 89–103. https://doi.org/10.1016/j.revpalbo.2003.12.003

Gill, B. C., Lyons, T. W., & Jenkyns, H. C. (2011). A global perturbation to the sulfur cycle during the Toarcian Oceanic Anoxic Event. *Earth and Planetary Science Letters*, *312*(3–4), 484–496. https://doi.org/10.1016/j.epsl.2011.10.030

Gill, B. C., Lyons, T. W., & Saltzman, M. R. (2007). Parallel, high-resolution carbon and sulfur isotope records of the evolving Paleozoic marine sulfur reservoir. *Paleogeography, Paleoclimatology, Paleoecology*, *256*(3–4), 156–173. https://doi.org/10.1016/j.palaeo.2007.02.030

Gill, B. C., Lyons, T. W., Young, S. A., Kump, L. R., Knoll, A. H., & Saltzman, M. R. (2011). Geochemical evidence for widespread euxinia in the later Cambrian ocean. *Nature*, *469*(7328), 80–83. https://doi.org/10.1038/nature09700

Hartke, E. M., Cramer, B. D., Calner, M., Melchin, M. J., Barnett, B. A., Orborny, S. C., & Bancroft, A. M. (2021). Decoupling $\delta^{13}C_{carb}$ and $\delta^{13}C_{org}$ at the onset of the Ireviken Excursion: $\delta^{13}C$ and organic carbon burial (f_{org}) during a Silurian oceanic anoxic event. *Global and Planetary Change*, *196*, 103373. https://doi.org/10.1016/j.gloplacha.2020.103373

Hayes, J. M., Strauss, H., & Kaufman, A. J. (1999). The abundance of ^{13}C in marine organic matter and isotopic fractionation in the global biogeochemical cycle of carbon during the past 800 Ma. *Chemical Geology*, *161*(1–3), 103–125. https://doi.org/10.1016/S0009-2541(99)00083-2

Jeppsson, L. (1987). Lithological and conodont distributional evidence for episodes of anomalous oceanic conditions during the Silurian. In R. J. Aldridge (Ed.), *Paleobiology of conodonts* (pp. 129–145). Ellis Horwood.

Jeppsson, L. (1990). An oceanic model for lithological and faunal changes tested on the Silurian record. *Journal of the Geological Society*, *147*(4), 663–674. https://doi.org/10.1144/gsjgs.147.4.0663

Jeppsson, L. (1997a). The anatomy of the mid-Early Silurian Ireviken Event. In C. Brett & G. C. Baird (Eds.), *Paleontological events: Stratigraphic, ecological, and evolutionary implications* (pp. 451–492). Columbia University Press.

Jeppsson, L. (1997b). A new latest Telychian, Sheinwoodian and Early Homerian (Early Silurian) standard conodont zonation. *Transactions of the Royal Society of Edinburgh: Earth-Science Reviews*, *88*(2), 91–114. https://doi.org/10.1017/S0263593300006854

Jeppsson, L., Eriksson, M. E., & Calner, M. (2006). A latest Llandovery to latest Ludlow high-resolution biostratigraphy based on the Silurian of Gotland—A summary. *GFF*, *128*(2), 109–114. https://doi.org/10.1080/11035890601282109

Kaljo, D., Kiipli, T., & Martma, T. (1997). Carbon isotope event markers through the Wenlock-Pridoli sequence at Ohesaare (Estonia) and Priekule (Latvia). *Paleogeography, Paleoclimatology, Paleoecology*, *132*(1–4), 211–223. https://doi.org/10.1016/s0031-0182(97)00065-5

Kampschulte, A., Bruckschen, P., & Strauss, H. (2001). The sulfur isotopic composition of trace sulfates in carboniferous brachiopods: Implications for coeval seawater, correlation with other geochemical cycles and isotope stratigraphy. *Chemical Geology*, *175*(1–2), 149–173. https://doi.org/10.1016/S0009-2541(00)00367-3

Kampschulte, A., & Strauss, H. (2004). The sulfur isotopic evolution of Phanerozoic seawater based on the analysis of structurally substituted sulfate in carbonates. *Chemical Geology*, *204*(3–4), 255–286. https://doi.org/10.1016/j.chemgeo.2003.11.013

Kiipli, T., Männik, P., Batchelor, R. A., Kiipli, E., Kallaste, T., & Perens, H. (2001). Correlation of Telychian (Silurian) altered volcanic ash beds in Estonia, Sweden and Norway. *Norwegian Journal of Geology*, *81*, 179–194.

Kump, L. R., & Arthur, M. A. (1999). Interpreting carbon-isotope excursions: Carbonates and organic matter. *Chemical Geology*, *161*(1–3), 181–198. https://doi.org/10.1016/S0009-2541(99)00086-8

Labandeira, C. C. (2005). Invasion of the continents: Cyanobacterial crusts to tree-inhabiting arthropods. *Trends in Ecology & Evolution*, *20*(5), 253–262. https://doi.org/10.1016/j.tree.2005.03.002

Lehnert, O., Männik, P., Joachimski, M. M., Calner, M., & Frýda, J. (2010). Paleoclimate perturbations before the Sheinwoodian glaciation: A trigger for extinctions during the "Ireviken Event". *Paleogeography, Paleoclimatology, Paleoecology*, *296*(3–4), 320–331. https://doi.org/10.1016/j.palaeo.2010.01.009

Lowenstein, T. K., Hardie, L. A., Timofeeff, M. N., & Demicco, R. V. (2003). Secular variation in seawater chemistry and the origin of calcium chloride basinal brines. *Geology*, *31*(10), 857–860. https://doi.org/10.1130/G19728R.1

Lyons, T. W., Gill, B. C., Shim, M. J., Frank, T. D., Hurtgen, M. T., Saltzman, M. R., et al. (2004). Carbonate associated sulfate as a paleoceanographic proxy: An update. *Geochimica et Cosmochimica Acta*, *68*(Suppl), A337.

Makhnach, A. A., Kruchek, S. A., Pokrovsky, B. G., Strel'tsova, G. D., Murashko, O. V., & Petrov, O. L. (2016). Carbon, oxygen, and sulfur isotope compositions and model of the Silurian rock formation in Northwestern Belarus. *Lithology and Mineral Resources*, *53*(1), 1–13. https://doi.org/10.1134/S0024490218010054

Männik, P., Loydell, D. K., Nestor, V., & Nõlvak, J. (2015). Integrated Upper Ordovician-lower Silurian biostratigraphy of the Grötlingbo-1 core section, Sweden. *GFF*, *137*(3), 226–244. https://doi.org/10.1080/11035897.2015.1042032

Marenco, P. J., Corsetti, F. A., Hammond, D. E., Kaufman, A. J., & Bottjer, D. J. (2008). Oxidation of pyrite during extraction of carbonate associated sulfate. *Chemical Geology*, *247*(1–2), 124–132. https://doi.org/10.1016/j.chemgeo.2007.10.006

McAdams, N. E. B., Cramer, B. D., Bancroft, A. M., Melchin, M. J., Devera, J. A., & Day, J. E. (2019). Integrated $\delta^{13}C_{carb}$, conodont, and graptolite biochemostratigraphy of the Silurian from the Illinois Basin and stratigraphic revision of the Bainbridge Group. *GSA Bulletin*, *131*(1–2), 335–352. https://doi.org/10.1130/B32033.1

Melchin, M. J., Sadler, P. M., & Cramer, B. D. (2020). Chapter 21: The Silurian Period. In F. M. Gradstein, J. G. Ogg, M. D. Schmitz, & G. M. Ogg (Eds.), *Geologic time scale 2020* (Vol. 2, pp. 695–732). Elsevier. https://doi.org/10.1016/B978-0-12-824360-2.00021-8

Munnecke, A., Calner, M., Harper, D. A., & Servais, T. (2010). Ordovician and Silurian sea-water chemistry, sea level, and climate: A synopsis. *Paleogeography, Paleoclimatology, Paleoecology*, *296*(3–4), 389–413. https://doi.org/10.1016/j.palaeo.2010.08.001

Munnecke, A., Samtleben, C., & Bickert, T. (2003). The Ireviken Event in the lower Silurian of Gotland, Sweden—Relation to similar Paleozoic and Proterozoic events. *Paleogeography, Paleoclimatology, Paleoecology*, *195*(1–2), 99–124. https://doi.org/10.1016/s0031-0182(03)00304-3

Oborny, S. C., Cramer, B. D., Brett, C. E., & Bancroft, A. M. (2020). Integrated Silurian conodont and carbonate carbon isotope stratigraphy of the east-central Appalachian Basin. *Paleogeography, Paleoclimatology, Paleoecology*, *554*, 109815. https://doi.org/10.1016/j.palaeo.2020.109815

Paytan, A., Yao, W., Faul, K. L., & Gray, E. T. (2020). Chapter 9: Sulfur isotope stratigraphy. In F. M. Gradstein, J. G. Ogg, M. D. Schmitz, & G. M. Ogg (Eds.), *Geologic time scale 2020* (Vol. 1, pp. 309–343). Elsevier. https://doi.org/10.1016/B978-0-12-824360-2.00009-7

Present, T. M., Gutierrez, M., Paris, G., Kerans, C., Grotzinger, J. P., & Adkins, J. F. (2019). Diagenetic controls on the isotopic composition of carbonate-associated sulfate in the Permian Capitan Reef Complex, West Texas. *Sedimentology*, *66*(7), 2605–2626. https://doi.org/10.1111/sed.12615

Present, T. M., Paris, G., Burke, A., Fischer, W. W., & Adkins, J. F. (2015). Large carbonate associated sulfate isotopic variability between brachiopods, micrite, and other sedimentary components in Late Ordovician strata. *Earth and Planetary Science Letters*, *432*, 187–198. https://doi.org/10.1016/j.epsl.2015.10.005

Raven, M. R., Fike, D. A., Bradley, A. S., Gomes, M. L., Owens, J. D., & Webb, S. A. (2019). Paired organic matter and pyrite $\delta^{34}S$ records reveal mechanisms of carbon, sulfur, and iron cycle disruption during ocean anoxic event 2. *Earth and Planetary Science Letters*, *512*, 27–38. https://doi.org/10.1016/j.epsl.2019.01.048

Richardson, J. A., Keating, C., Lepland, A., Hints, O., Bradley, A. S., & Fike, D. A. (2019). Silurian records of carbon and sulfur cycling from Estonia: The importance of depositional environment on isotopic trends. *Earth Planet Science Letters*, *512*, 71–82. https://doi.org/10.1016/j.epsl.2019.01.055

Richardson, J. A., Lepland, A., Hints, O., Prave, A. R., Gilhooly, W. P., III., Bradley, A. S., & Fike, D. A. (2021). Effects of early marine diagenesis and site-specific depositional controls on carbonate-associated sulfate; insights from paired S and O isotopic analyses. *Chemical Geology*, *584*, 120525. https://doi.org/10.1016/j.chemgeo.2021.120525

Rose, C. V., Fischer, W. W., Finnegan, S., & Fike, D. A. (2019). Records of carbon and sulfur cycling during the Silurian Ireviken Event in Gotland, Sweden. *Geochimica et Cosmochimica Acta*, *246*, 299–316. https://doi.org/10.1016/j.gca.2018.11.030

Saltzman, M. R., Young, S. A., Kump, L. R., Gill, B. C., Lyons, T. W., & Runnegar, B. N. (2011). Pulse of atmospheric oxygen during the late Cambrian. *Proceedings of the National Academy of Sciences of the United States of America*, *108*(10), 3876–3881. https://doi.org/10.1073/pnas.1011836108

Samtleben, C., Munnecke, A., Bickert, T., & Pätzold, J. (1996). The Silurian of Gotland (Sweden): Facies interpretation based on stable isotopes in brachiopod shells. *Geologische Rundschau*, *85*(2), 278–292. https://doi.org/10.1007/BF02422234

Scotese, C. R. (2014). Atlas of Silurian and Middle-Late Ordovician paleogeographic maps (Mollweide Projection), Maps 73-80, Volume 5, the Early Paleozoic, PALEOMAP Atlas for ArcGIS, PALEOMAP Project, Evanston, IL.

Servais, T., Owen, A. W., Harper, D. A. T., Kröger, B., & Munnecke, A. (2010). The Great Biodiversification Event (GOBE): The paleoecological dimension. *Paleogeography, Paleoclimatology, Paleoecology*, *294*(3–4), 99–119. https://doi.org/10.1016/j.palaeo.2010.05.031

Sim, M. S., Ono, S., Donovan, K., Templer, S. P., & Bosak, T. (2011). Effect of electron donors on the fractionation of sulfur isotopes by a marine *Desulfovibrio* sp. *Geochimica et Cosmochimica Acta*, *75*(15), 4244–4259. https://doi.org/10.1016/j.gca.2011.05.021

Stolfus, B. M., Allman, L. J., Young, S. A., Calner, M., Hartke, E. R., Oborny, S. C., et al. (2022). Sulfur isotope data (CAS and Py) from the Altajme core, Gotland, Sweden, (Version 1.0) [Dataset]. Interdisciplinary Earth Data Alliance (IEDA). https://doi.org/10.26022/IEDA/112299

Strauss, H. (1999). Geological evolution from isotope proxy signals–sulfur. *Chemical Geology*, *161*(1–3), 89–101. https://doi.org/10.1016/S0009-2541(99)00082-0

Swart, P. K., & Oehlert, A. M. (2018). Revised interpretations of stable C and O patterns in carbonate rocks resulting from meteoric diagenesis. *Sedimentary Geology*, *364*, 14–23. https://doi.org/10.1016/j.sedgeo.2017.12.005

Toyama, K., Paytan, A., Sawada, K., & Hasegawa, T. (2020). Sulfur isotope ratios in co-occurring barite and carbonate from Eocene sediments: A comparison study. *Chemical Geology*, *535*, 119454. https://doi.org/10.1016/j.sedgeo.2017.12.005

Vandenbroucke, T. R., Emsbo, P., Munnecke, A., Nuns, N., Duponchel, L., Lepot, K., et al. (2015). Metal-induced malformations in early Paleozoic plankton are harbingers of mass extinction. *Nature Communications*, *6*(1), 1–7. https://doi.org/10.1038/ncomms8966

Vandenbroucke, T. R., Munnecke, A., Leng, M. J., Bickert, T., Hints, O., Gelsthorpe, D., et al. (2013). Reconstructing the environmental conditions around the Silurian Ireviken Event using carbon isotope composition of bulk and palynomorph organic matter. *Geochemistry, Geophysics, Geosystems*, *14*(1), 86–101. https://doi.org/10.1029/2012GC004348

Webby, B. D., Droser, M. L., Paris, F., & Percival, I. G. (2004). *The Great Ordovician Biodiversification Event* (p. 484). Columbia University Press.

Wenzel, B., & Joachimski, M. M. (1996). Carbon and oxygen isotopic composition of Silurian brachiopods (Gotland/Sweden): Paleoceanographic implications. *Paleogeography, Paleoclimatology, Paleoecology*, *122*(1–4), 143–166. https://doi.org/10.1016/0031-0182(95)00094-1

Wortmann, U. G., & Paytan, A. (2012). Rapid variability of seawater chemistry over the past 130 Myr. *Science*, *337*(6092), 334–336. https://doi.org/10.1126/science.1220656

Wotte, T., Shields-Zhou, G. A., & Strauss, H. (2012). Carbonate-associated sulfate: Experimental comparisons of common extraction methods and recommendations toward a standard analytical protocol. *Chemical Geology*, *326*, 132–144. https://doi.org/10.1016/j.chemgeo.2012.07.020

Yao, W., Paytan, A., Griffith, E. M., Martínez-Ruiz, F., Markovic, S., & Wortmann, U. G. (2020). A revised seawater sulfate S-isotope curve for the Eocene. *Chemical Geology*, *532*, 119382. https://doi.org/10.1016/j.chemgeo.2019.119382

Yao, W., Wortmann, U. G., & Paytan, A. (2019). Sulfur isotopes—Use for stratigraphy during times of rapid perturbation. *Stratigraphy and Timescales*, *4*, 1–33. https://doi.org/10.1016/bs.sats.2019.08.004

Young, S. A., Benayoun, E., Kozik, N. P., Hints, O., Martma, T., Bergström, S. M., & Owens, J. D. (2020). Marine redox variability from Baltica during extinction events in the latest Ordovician-early Silurian. *Paleogeography, Paleoclimatology, Paleoecology*, *554*, 1–17. https://doi.org/10.1016/j.palaeo.2020.109792

Young, S. A., Kleinberg, A., & Owens, J. D. (2019). Geochemical evidence for expansion of marine euxinia during an early Silurian (Llandovery-Wenlock boundary) mass extinction. *Earth Planet Science Letters*, *513*, 187–196. https://doi.org/10.1016/j.epsl.2019.02.023